10.21608/avmj.2025.380937.1687 Assiut University web-site: www.aun.edu.eg

EVALUATING THE AMELIORATIVE EFFECT OF MSCS AND EXOSOMES ON MWCNTS LUNG TOXICITY USING HISTOPATHOLOGY AND MORPHOMETRY IN RATS

NOHAIR A. MOHAMED [1], EL-BEGAWEY M.B.[1], WALAA A. MOSELHY [2], DOAA R.I. ABDEL-GAWAD [2] AND EL-SHAYMAA EL-NAHASS [1]

[1] Veterinary Pathology Department, Faculty of Veterinary Medicine, Beni-Suef University, Beni-Suef, Egypt.
[2] Toxicology and Forensic Medicine Department, Faculty of Veterinary Medicine, Beni-Suef University, Beni-Suef, 62511, Egypt.

Received: 4 May 2025; **Accepted:** 16 June 2025

ABSTRACT

The growing use of multi-walled carbon nanotubes (MWCNTs) in industry and medicine has raised concerns about their potential toxicity to human and animal health, particularly their ability to cause oxidative stress, inflammation, and fibrosis. Mesenchymal stem cells (MSCs) and their exosomes have emerged as promising therapeutic agents due to their effective immunomodulatory, anti-inflammatory, and antioxidant properties. Herein, we investigate the effects of MSCs and MSC-derived exosomes against MWCNTs-induced pulmonary toxicity in albino rats. Thirty-two male rats (4 weeks old) were divided into four groups: (1) a control group receiving normal saline, (2) an MWCNTs-exposed group administered MWCNTs (1 mg/kg BW, intraperitoneally (IP), twice at the first and third weeks), (3) an MWCNTs + MSCs + exosomes-treated group receiving MWCNTs (1 mg/kg BW, IP) followed by MSCs (2.5×10^6 cells/kg BW, IP) and exosomes (100 µg MSC-EV protein/kg BW, IP) weekly for three weeks, and (4) an MSCs + exosomes-only group receiving the same MSC and exosome doses without MWCNT exposure. MWCNTs exposure resulted in a significant increase in bronchiolar epithelial thickness, goblet cell hyperplasia, elevated fibrosis levels (Masson's trichrome staining), and increased oxidative stress markers, including malondialdehyde (MDA). These effects were mitigated by MSCs and exosomes through reducing epithelial thickening and goblet cell hyperplasia, decreasing fibrosis, and restoring antioxidant markers such as glutathione (GSH). Histopathological analysis confirmed lung regeneration by decreasing inflammation, degeneration, and fibrosis. These findings highlight the therapeutic potential of MSC-based therapy and the value of digital pathology tools like ImageJ in nanotoxicology research.

Keywords: Image J, MWCNTs, MSC-derived Exosomes, Morphometric Analysis, Pulmonary Toxicity

INTRODUCTION

A novel way to histological research has been made possible by digital Pathology and image analysis, enabling morphometric evaluation on whole slide imaging (WSI) through specialized computational tools (Dero Ulers *et al.,* 2013; Hamilton *et al.,* 2014; Griffin and Treanor, 2017; Aeffner *et al.,* 2019; Liu and Pantanowitz, 2019; Jahn *et al.,* 2020; Nam *et al.,* 2020; Pallua *et al.,* 2020). One of these

Corresponding author: NOHAIR A. MOHAMED
E-mail: nohairmohamed841_sd@vet.b-su.edu.eg
Present address: Veterinary Pathology Department, Faculty of Veterinary Medicine, Beni-Suef University, Beni-Suef, Egypt.

tools is ImageJ, a tool that uses Java and open-source software and is free. ImageJ has gained widespread use in biological research and was developed by the National Institutes of Health (NIH). It allows for morphometric analysis of stained histological sections through the use of plug-ins and macros that can be downloaded (Girish & Vijayalakshmi, 2024). Rich online resources (https://imagej.net/ij) facilitate diverse applications, such as nuclear morphology assessment, cell counting, area measurement, tumor heterogeneity analysis, and quantitative immunohistochemistry (Hamilton *et al.,* 2014; Nast *et al.,* 2015; Madabhushi and Lee, 2016; Aeffner *et al.,* 2017). Combined Masson's trichrome staining with morphometry is a practical way to measure collagen fibers and assess epidermal thickness, hyperkeratosis, and parakeratosis (Flotte *et al.,* 1989; Miot *et al.,* 2007; Hong *et al.,* 2020).

Carbon nanotubes (CNTs) are nanomaterials made of carbon and made up of hollow tubes. They can be classified into single-walled (SWCNTs) and multi-walled (MWCNTs) and have diameters ranging from 0.8–2 nm and 10–11 nm, respectively (Abu Gazia & El-Magd, 2018; Öner *et al.,* 2018). Because of their unique physicochemical properties and biocompatibility, CNTs are widely applied in medicine and industry (Ali *et al.,* 2020). The use of these devices for delivering chemotherapeutic agents targeting cancer cells has been investigated, along with gene therapy vectors (Cifuentes-Rius *et al.,* 2017) and vaccine delivery platforms that enhance antibody responses (Witkowska *et al.,* 2022). Despite their benefits, prolonged exposure to CNTs raises concerns regarding potential toxicity, including oxidative stress-induced cytotoxicity, genotoxicity, and inflammatory responses (Madannejad *et al.,* 2019).

Multiple studies have established that CNTs exhibit detrimental effects on animal tissues, which cause their accumulation in the liver, kidneys, lungs, and brain after exposure, according to Mercer *et al.* (2013).

MWCNTs serve as a causative factor behind several forms of toxicity, including allergies and pulmonary toxicity, as well as hepatotoxicity, fibrosis, neurotoxicity, and nephrotoxicity (Talkar *et al.,* 2018). The research demonstrates that exposure conditions play a crucial role in causing neurotoxic damage in mice, while also causing kidney damage related to oxidative stress (Abu Gazia & El-Magd, 2019; Zamani *et al.,* 2021; Sallam *et al.,* 2022). MWCNTs reach vulnerable lung tissue through their small dimensions because they access alveolar spaces as well as interstitial tissue and pleural regions, causing inflammation along with interstitial fibrosis and bronchiolar and alveolar hypertrophy and granuloma formation (Wynn, 2011; Czarny *et al.,* 2014; Kobler *et al.,* 2015; Jacobsen *et al.,* 2016; Poulsen *et al.,* 2016). The use of CNTs for intraperitoneal administration creates multiple toxicology-related concerns because it has the potential to cause cancer, together with other unknown negative effects (Madani *et al.,* 2013; Visalli *et al.,* 2019).

The leading medical field of cell therapy presents MSCs as one of its most significant prospects, according to research done by Aijaz *et al.* (2018). The preliminary discovery of MSCs occurred through Friedenstein *et al.* (1966), who established that these cells can develop into cells of mesodermal, endodermal, and neuroectodermal origin (Kopen *et al.,* 1999; Petersen *et al.,* 1999; Pittenger *et al.,* 1999). Recently discovered MSC properties demonstrate immunomodulation capacity through the control of interleukin-10 (IL-10) and tumor necrosis factor (TNF) inhibition and actively prevent inflammation and assist neutrophil cell death (Aggarwal & Pittenger, 2005; Raffaghello *et al.,* 2007). Recent research has validated exosomes derived from MSCs (MSC-Exos) as therapeutic agents, because they present stability and immune regulation benefits,

together with regenerative properties, without any risk of tumor development (Mathivanan *et al.,* 2011; Zhang *et al.,* 2022). The cellular communication medium that exosomes represent measures between 40 and 150 nm in diameter to support disease treatments (Ma *et al.,* 2020; Wang *et al.,* 2020). The therapeutic effectiveness of MSC-Exos has verified benefits for medical conditions that affect the lungs, myocardium, kidneys, nerves, skin, and processes of aging, according to Ebrahim *et al.* (2018). The research study utilized ImageJ software to examine how MWCNTs cause harm to biological systems by inducing bronchiolar epithelium and goblet cell hyperplasia, together with fibrosis in lung tissue. Special staining approaches will reveal how MSCs, together with their exosomes, affect therapy to determine their protective abilities against MWCNT-induced cell and tissue harm.

MATERIALS AND METHODS

1. Materials

Unfunctionalized MWCNTs (dry powder, 95.07% by weight (96.96% atomic percentage) were purchased from the Egyptian Petroleum Research Institute (EPRI), Cairo, Egypt.

2. Characterization and preparation of MWCNTs

Scanning (SEM) and transmission (TEM) electron microscopy were used to determine MWCNTs shape, length, and mean diameter. Before injection, the test material was weighed and then dispersed in distilled water. Immediately prior to administration, the suspensions were sonicated for 10 min at a power setting of 3 using the Branson Sonifier 250 (Branson Ultrasonics Corp., USA).

2.1. High-resolution transmission electron microscopy (HRTEM) and field emission scanning electron microscopy (FESEM)

To evaluate the surface morphology and particle size of the prepared sample, CNTs was investigated by high-resolution transmission electron microscopy (HRTEM) using (JEM. 100 CX11, Electron Microscope Unit, Assiut University). Additionally, scanning electron microscopy (SEM) analysis was performed with a field emission scanning electron microscope (FESEM) using a Philips-XL30 device (The Netherlands) equipped with energy-dispersive X-ray (EDX) microanalysis hardware.

2.2. X-ray diffraction (XRD)

X-ray diffraction (XRD**)** patterns were determined using a Panalytical (Empyrean) X-ray diffractometer system at 40 kV and 35 mA with monochromatized Cu Kα radiation (λ = 1.5406 Å) and a scanning speed of 2 per min (step size = 0.050 and step time = 1.5 s). The scanning range (2θ scale) was within 5-80.

2.3. Mesenchymal stem cells and exosomes:

3.1. Isolation of Mesenchymal stem cells from Wharton Jelly (Isolation of WJ-MSCs):

Isolation of MSCs was established using the explant method as previously described (Almaeen *et al.,* 2025)

MSCs were isolated from five umbilical cords obtained from healthy cesarean deliveries with informed consent. Wharton's jelly was dissected, scraped, and cultured in flasks. After a 2-hour adhesion period, a complete medium (Dulbecco's Modified Eagle's Medium DMEM + 20% fetal bovine serum (FBS), 100 µL penicillin, 100 µL streptomycin, 20 µL fungizone) was added. Cultures were maintained at 37 °C in a CO_2 incubator, with medium changes every 3 days. Tissue remnants were removed after 5–6 days. At 90% confluence, cells were harvested using 0.05% trypsin-EDTA (Euroclone, Italy).

Morphological assessment was performed, and MSCs identity was confirmed based on the International Society for Cellular Therapy (ISCT) criteria: 1. Plastic adherent 2. Fibroblast morphology 3. Surface expression: positive for CD105, CD73, and CD90, and negative for CD45, CD34, CD14, CD11b, CD79alpha, CD19, and HLA-DR molecules 4. MSC differentiate to osteoblasts, adipose cells.

3.2. Characterization of human umbilical cord mesenchymal stem cells (hUC-MSCs) via flow cytometry analysis:

The adherent cells were detached and stained with phycoerythrin (PE)- or fluorescein isothiocyanate (FITC)-conjugated antibodies for cell surface antigen phenotype. Labeled cells were analyzed by the CytoFLEX, which utilizes cytexpert (Beckham Coulter Software) for CytoFLEX analysis.

3.3. Isolation of Exosomes from Mesenchymal stem cell culture:

Exosomes isolation was done using a differential, sequential centrifugation technique, according to (Gupta *et al.,* 2018).

3.4. Quantitation of exosome concentration:

Protein content is used for measuring exosome content. Trichloroacetic acid is used to precipitate exosomes. then kept suspended in a buffer of known volume. The Bradford test is used to evaluate protein content. A concentration of 20–30 ug/ml of exosomes was suspended for injection in sterile saline.

4. Chemicals

Chemicals used for the estimation of oxidant/antioxidant biomarkers were purchased from Loba-chemie Co. (Mumbai, Maharashtra, India) and Carl Roth-Germany.

5. Experimental design:

protocol was approved by the Institutional Animal Care and Use Committee of Beni-Suef University (BSU-IACUC, approval no. 022-312). Thirty-two (32) male albino rats (4 weeks old, 110.0 ± 10 g) were obtained from the Animal House, Faculty of Pharmacy, Nahda University, Egypt. Animals were housed under controlled conditions (25°C, standard humidity) with free access to food and water and acclimatized for one week prior to the experiment. Rats were randomly divided into four equal groups (n=8): Group 1 (Control): Received intraperitoneal (IP) injections of saline (0.5 ml/rat) once weekly. Group 2 (MWCNTs): Received IP injections of MWCNTs at a dose of 1 mg/kg body weight (0.5 ml/rat) during the 1st and 3rd weeks (Sakamoto *et al.,* 2018). Group 3 (MWCNTs + MSCs + Exosomes): Received the same MWCNTs dose as G2, along with weekly IP injections of MSCs and exosomes during the 2nd, 3rd and 4th weeks. MSCs were administered at 2.5 million cells/kg BW (0.5 ml/rat), and exosomes at 100 µg protein/kg BW (0.5 ml/rat). Group 4 (MSCs + Exosomes): Treated similarly to G3, but without MWCNT exposure. Before injection, MWCNTs were sonicated for 10 minutes using the Branson Sonifier 250 (Branson Ultrasonics Corp., USA) at a power setting of 3. An illustration of the experimental groups and protocol is provided in Figure 1.

6. Sampling

At the end of the experiment (day 30), rats were euthanized by cervical dislocation. After dissection, lung tissues were immediately removed, weighed, and washed with phosphate-buffered saline (PBS) to remove blood. Lung specimens were divided into 3 parts. The first part was preserved in 10% formalin (for histopathology). The second part was kept at 80 °C (for real-time PCR). The third part was homogenized with PBS, centrifuged (10,000 g/15 min/4 °C), and the supernatant was kept at 20 °C (for tissue biochemical assay).

7. Methodology

7.1. Estimation of oxidant/antioxidant biomarkers

By using spectrophotometric technical methods, we determine oxidative stress biomarkers in lung tissue homogenates. To determine levels of reduced glutathione (GSH), we used a previously reported method by Ellman (1959) with the modification of protein precipitation using trichloroacetic acid (TCA), as described by Sedlak and Lindsay (1968). Malondi-aldehyde (MDA) levels were measured following the method of Jensen et al. (1997), while the total thiol concentrations were evaluated using the Ellman (1959) method. Protein thiols were quantified by subtracting NP-SH concentrations from total sulfhydryl (T-SH) content, following the approach summed up by Sedlak and Lindsay (1968).

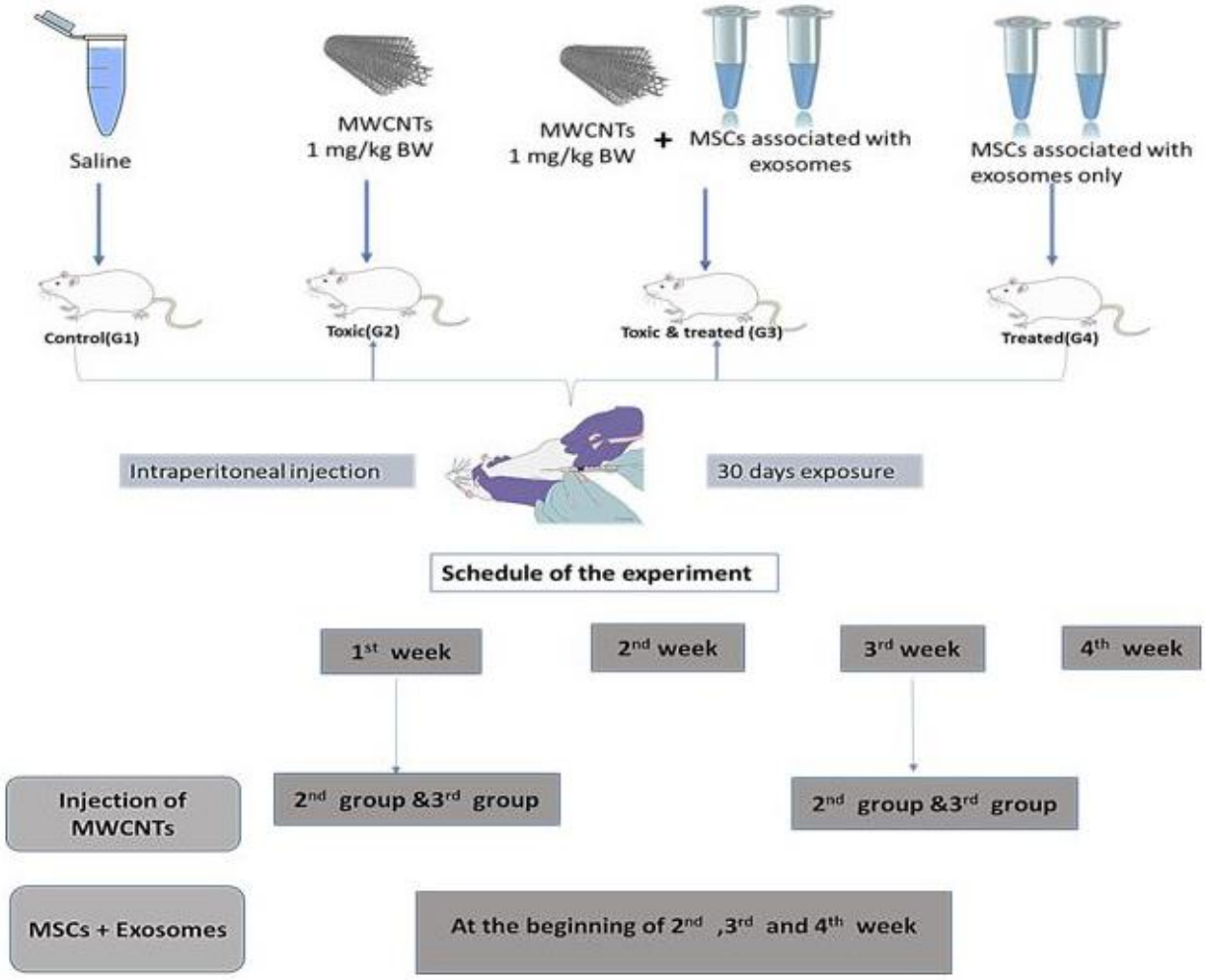

Fig. 1: Illustration of experimental design and animals grouping.

7.2. Histological Analyses

The tissues were fixed in 10% buffered formalin for 24 hours. Representative tissue sections were placed in histopathological cassettes. The tissue was gradually dehydrated through a series of ethyl alcohol solutions with increasing concentrations until reaching pure, water-free alcohol. Subsequently, the tissue was cleared in xylene, embedded in paraffin, and blocked. Tissue blocks were cut into 3–5 µm-thick sections using a rotary microtome, placed on slides, and stained with hematoxylin and eosin stain (H&E), following routine protocols as outlined by Bancroft & Layton (2019). The stained sections were examined under a light microscope, and a digital camera (DM2500 M; Leica, Germany) was used to examine and photograph the lesions.

7.2. A. Masson's Trichrome Staining

The tissue sections were prepared for Masson's trichrome staining through removal of paraffin and then hydration before being refixed with Bouin's solution, according to Royce *et al.* (2013). Muscle fibers received Biebrich scarlet-acid fuchsin stain together with cytoplasm, whereas Weigert's iron hematoxylin served for staining nuclear structures. The tissue differentiating agent comprising phosphor-molybdic-phosphotungstic acid was applied before aniline blue stained the collagen fibers. The process of final differentiation included treatment with 1% acetic acid until completion, before the steps of clearing and mounting (Suvarna, Layton, & Bancroft, 2019).

7.2.B. Periodic acid–Schiff (PAS) staining

The tissue section dewaxing process commenced through xylene treatment, before sections moved through gradually increasing concentrations of ethanol for rehydration. During the reaction process, periodic acid oxidized the sections, while water provided extensive rinses. Clinical use of Schiff reagent for the following treatment step was followed by a tap water rinse and then dehydration of the samples. The clearing process for dehydrated sections followed the protocol described in Suvarna, Layton & Bancroft (2019).

7.3. Morphometrical Image analysis

Lung sections were examined and photographed using a digital camera (DM2500 M; Leica, Germany) and a freeware version of ImageJ 1.53k, downloaded from the National Institutes of Health website (https://imagej.net/ij). Parameters selected for morphometric analysis included area, area fraction, minimum and maximum gray values, perimeter, length, and integrated density. These parameters were measured within a standard measuring frame of a known area, using 50 captured images per slide at 200x magnification under 20x lens. The slides were routinely stained with hematoxylin-eosin (HE) and additionally stained with Masson's trichrome and PAS. Before conducting the measurements, the scale was calibrated to micrometers using the set scale function in ImageJ, as described by (El-Nahass *et al.,* 2017).

7.3.A. Quantification of Fibrosis in Bronchial Tissue& Area Percentages

Masson's trichrome-stained sections were used to estimate equivalent fibrosis in the bronchial tissue using Image J software. The images were first converted to grayscale, and the HSB (brightness, saturation and hue) stack splitter was used to split the colored image into three slices, which were brightness, saturation and hue as shown in (Fig.2). The hue stacks were used to determine the fibrotic area. The fibrotic areas were binarized with a red threshold to include all the fibrotic areas. Based on a morphological analysis of sections at 200x magnification, the fibrotic area was quantified as a percentage of the total bronchial tissue area. This methodology is based on previously used procedures to study dermal collagen content, as described by El-Nahass *et al. (*2017).

7.3.B. Measurement of the thickness of bronchiolar epithelium

Bronchial epithelial thickness was assessed using (H&E) stained sections and determined by initiating a perpendicular line (blue line) from the basement membrane to the surface of the epithelial layer at several different points, according to (Royce *et al.,* 2013b) as shown in (Fig.3). These measurements were taken in micrometers, and the wall thickness was corrected for variation within each sector of the bronchi by averaging values obtained from several regions.

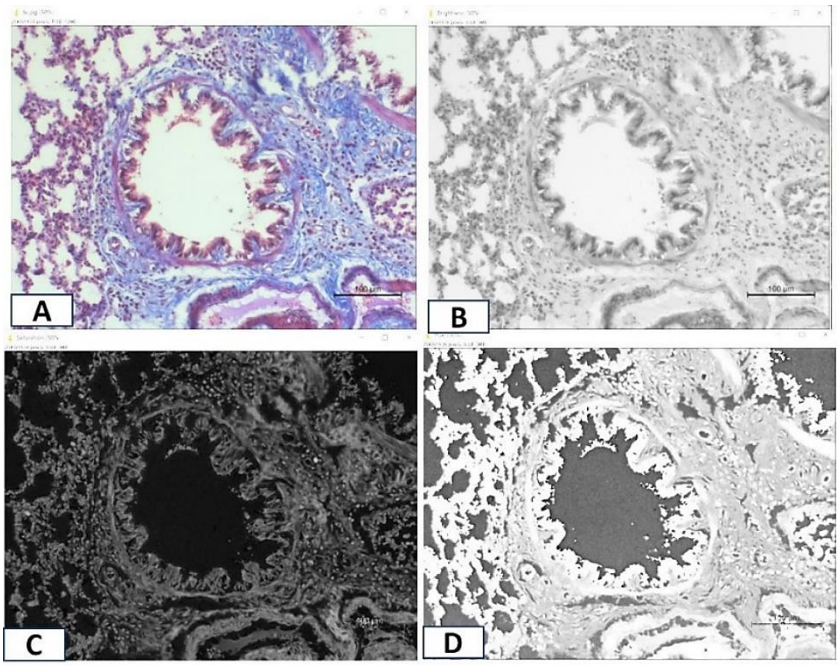

Fig. 2: Representative Masson-trichrome-stained sections (A-D) showing the image was converted to grayscale, and the HSB (A; original capture, B; brightness, C; saturation and D hue).

7.3.C. Goblet Cells Hyperplasia Integrated Density Area Percentages

Goblet cells were identified in PAS-stained lung sections by their magenta coloration due to mucin content. To quantify hyperplasia, images were converted to Hue-Saturation-Brightness (HSB) color space, separating them into three grayscale channels representing brightness, saturation and hue color space, as shown in Fig (4). The saturation stack was chosen, as it highlights the magenta-stained areas. A threshold was applied to detect positive regions, which were then masked in red binary. By using ImageJ, the area percentage and integrated density were measured with the corresponding options enabled, as described by El-Nahass *et al.* (2017). The area percentage was calculated relative to the total bronchial area, while the integrated density reflected the staining intensity, providing quantitative insight into the extent and severity of goblet cell hyperplasia.

8. Statistical Analysis

The data were analyzed using IBM SPSS version 26 statistical software to reveal significant differences between groups. A one-way analysis of variance (one-way ANOVA) was used, followed by a Tukey post-hoc test. The differences were considered statistically significant at $P<0.05$. The results were provided as mean ± standard deviation (SD).

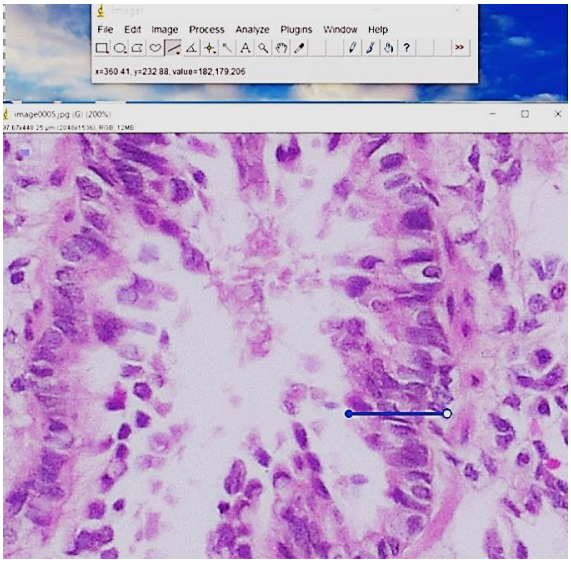

Fig. 3: Epithelial thickness was measured from the luminal surface of the epithelium to the basement membrane (blue line).

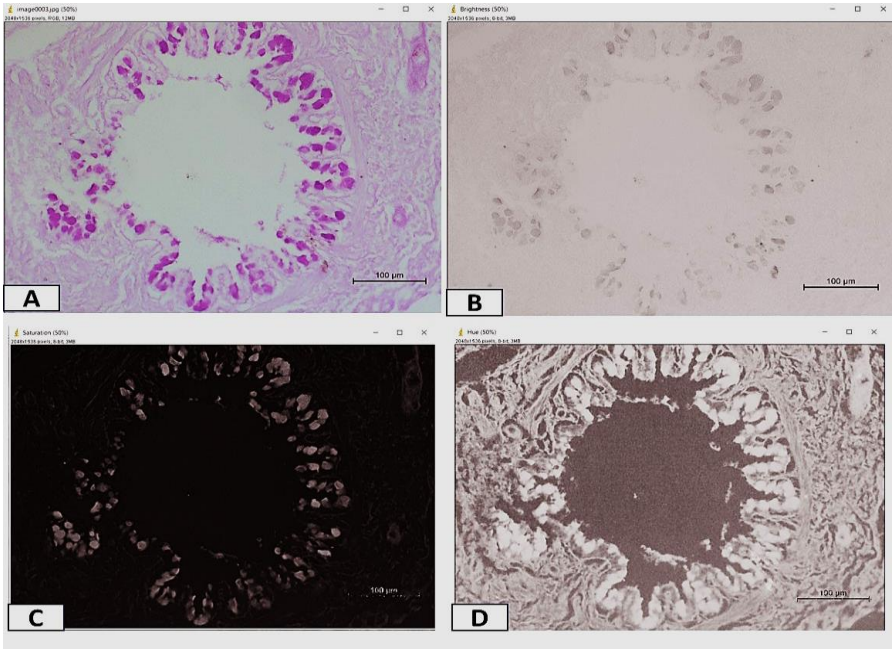

Fig. 4: Representative PAS-stained sections (A-D) showing the image was converted to grayscale, and the HSB (A; original capture, B; brightness, C; saturation and D hue).

RESULTS

3.1. Characterization of MWCNTs

The study uses electron microscope images to analyze carbon nanotubes (CNTs) for their structural integrity and quality. The TEM image shows a network of entangled, multi-walled nanotubes with a tubular morphology, indicating high structural integrity effective (Alosime, 2023) (Figure 5, A). The SEM image shows a complex network of intertwined carbon nanotubes with varying diameters, forming a dense mesh-like architecture. The EDX analysis reveals a composition dominated by carbon, with trace elements present (Figure 5, B). The carbon content is 95.07%, indicating successful synthesis of high-purity CNTs. The presence of oxygen suggests minor surface oxidation or functionalization (Figure 5, C1, C2).

The XRD pattern of carbon nanotubes shows three characteristic peaks, confirming the successful synthesis of multi-walled carbon nanotubes (MWCNTs). The most prominent peak is at 26° (2θ), representing the interlayer spacing between concentric graphitic layers. A broader peak at 43° (2θ) reflects the hexagonal arrangement of carbon atoms within the tube walls. The overall peak pattern, intensities, and positions are consistent with typical MWCNT structures (Fig.5).

3.2. Characterization of Mesenchymal stem cells:

3.2.1. Morphology of hUC-MSCs:

The obtained images via the inverted microscope showed small rounded cells at the beginning of culturing. With time, the cells expanded and became spindle-shaped cells exhibiting the fibroblast-like morphology and capability to form colonies (Fig 6 a& b).

3.2.2. Characterization of hUC-MSCs *via* flow cytometry analysis:

Figure (7) revealed that the cultured hUC-MSCs were expressed the surface markers CD34 and 45 negatively.

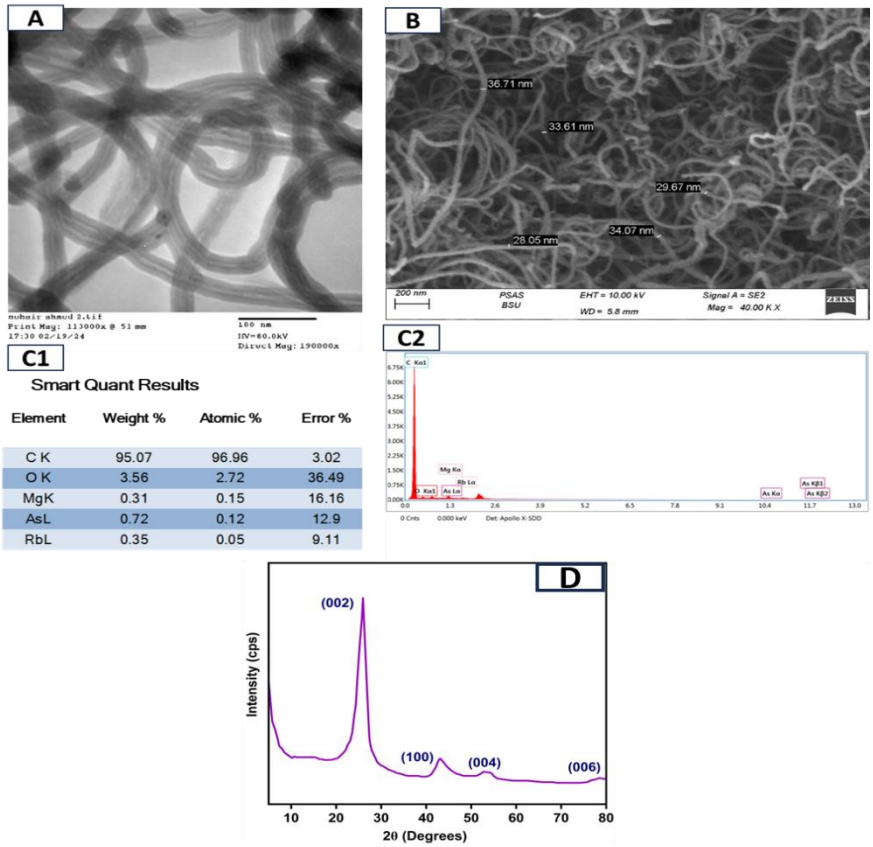

Fig. 5: Morphology and dimensional features of MWCNTs as revealed by transmission electron microscope (A) (Alosime, 2023b), scanning electron microscope (B and (C1, C2) EDX of MWCNTs and XRD of CNTs (D).

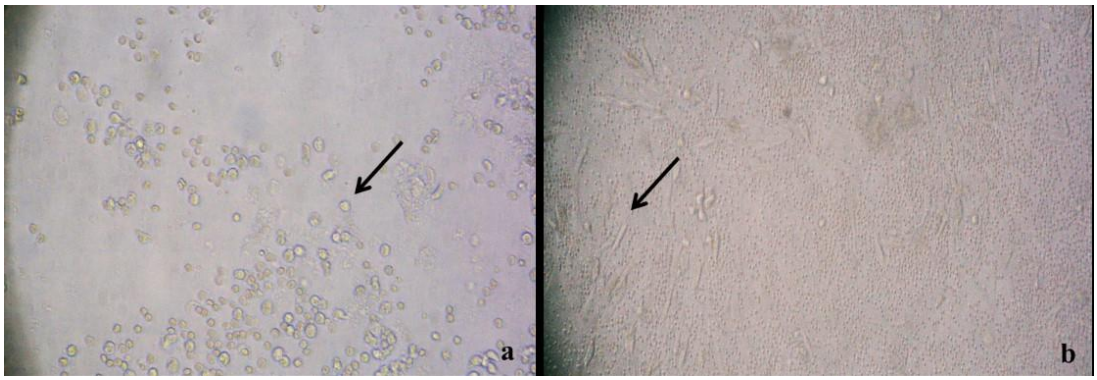

Fig. 6: (a&b): Morphology of the cultured hUC-MSCs a) small rounded cells at the second day, and b) spindle-shaped cells at the tenth day.

3.3. Histopathological findings

Histopathological analysis of lung tissues from the four experimental groups (G1–G4) revealed varying degrees of pathological changes, including lymphoid hyperplasia (peribronchiolar nodosa), epithelial hyperplasia, necrosis, degeneration, and alveolar wall thickening.

The control group (G1) exhibited normal pulmonary architecture, with well-preserved alveolar and bronchiolar structures. Mild pathological alterations were noted, including minimal peribronchiolar nodosa (+), epithelial hyperplasia (+), necrosis/degeneration (+), and mild alveolar wall thickening (+) (Fig. 8A).

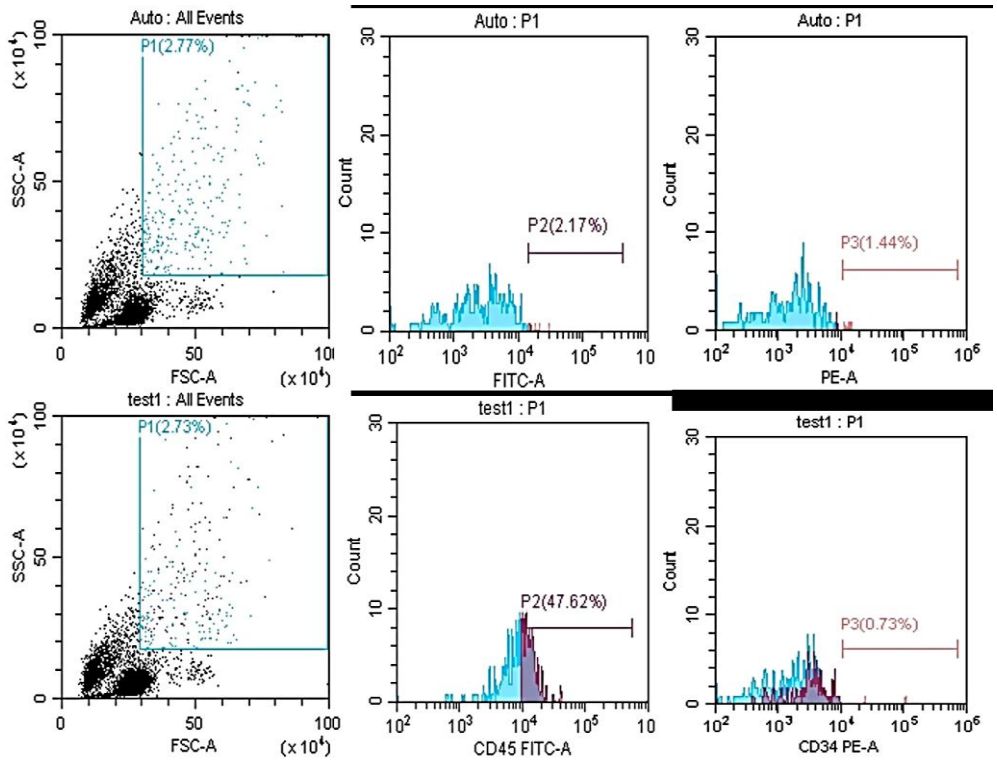

Fig. 7: The cultured hUC-MSCs were labeled with CD34 and CD45 antibodies against human antigens and showing negative expression.

In contrast, the MWCNT-exposed group (G2) displayed marked histopathological damage. Prominent peribronchiolar nodosa (++/+++) was observed, indicating extensive mononuclear cell infiltration and lymphoid hyperplasia. Epithelial hyperplasia was moderate to severe (++/+++), reflecting a strong proliferative response. Necrosis and degeneration were also elevated (++/+++), accompanied by marked vascular congestion and edema (Fig. 8B1). Alveolar wall thickening was moderate to severe (++/+++), suggesting significant parenchymal remodeling (Fig. 8B2). Numerous large, pale, foamy macrophages were present within alveolar spaces, either scattered or clustered (black arrow) (Fig. 8B3).

Group G3, which received MSC-exosome therapy following MWCNT exposure, showed moderate peribronchiolar nodosa (++), indicating a partial reduction in inflammation (Fig. 8C1). Epithelial hyperplasia was reduced to mild to moderate levels (+/++), while necrosis and degeneration were also decreased to mild levels (+). However, alveolar wall thickening remained severe (+++), indicating persistent structural remodeling (Fig. 8C2). Foamy macrophages were still evident in alveolar spaces (Fig. 8C2, inset).

The MSC-exosome-only group (G4) exhibited histological improvements comparable to, or slightly better than those in G3. Peribronchiolar nodosa was mild to moderate (+/++), with epithelial hyperplasia also reduced (+/++). Necrosis and degeneration were moderate (++), and alveolar wall thickening was likewise moderate (++), suggesting partial protection against fibrotic changes (Fig. 8D1, D2).

Lymphocytic aggregates of variable grades were observed across all groups, including the control group, where they appeared at low levels. These aggregates were predominantly located in perivascular or peribronchiolar regions and mainly composed of lymphocytes with hyper-chromatic nuclei and scant cytoplasm.

Table 1: The four histopathological parameters that were estimated in the lung.

Item	Peribronchiolar nodosa	Epithelium Hyperplasia	Necrosis /degeneration	thickness of alveolar walls
G1	+ (Mild)	+ (Mild)	+ Mild	+ Mild
G2	++/+++ (Moderate to severe)	++/+++ (Moderate to severe)	++/+++ (Moderate to severe)	++/+++ (Moderate to severe)
G3	++ (Moderate)	+/++ (Mild to Moderate)	+ (Mild)	(>+++) Very Severe
G4	+/++ (Mild to Moderate)	+/++ (Mild to Moderate)	++ (Moderate)	++ (Moderate)

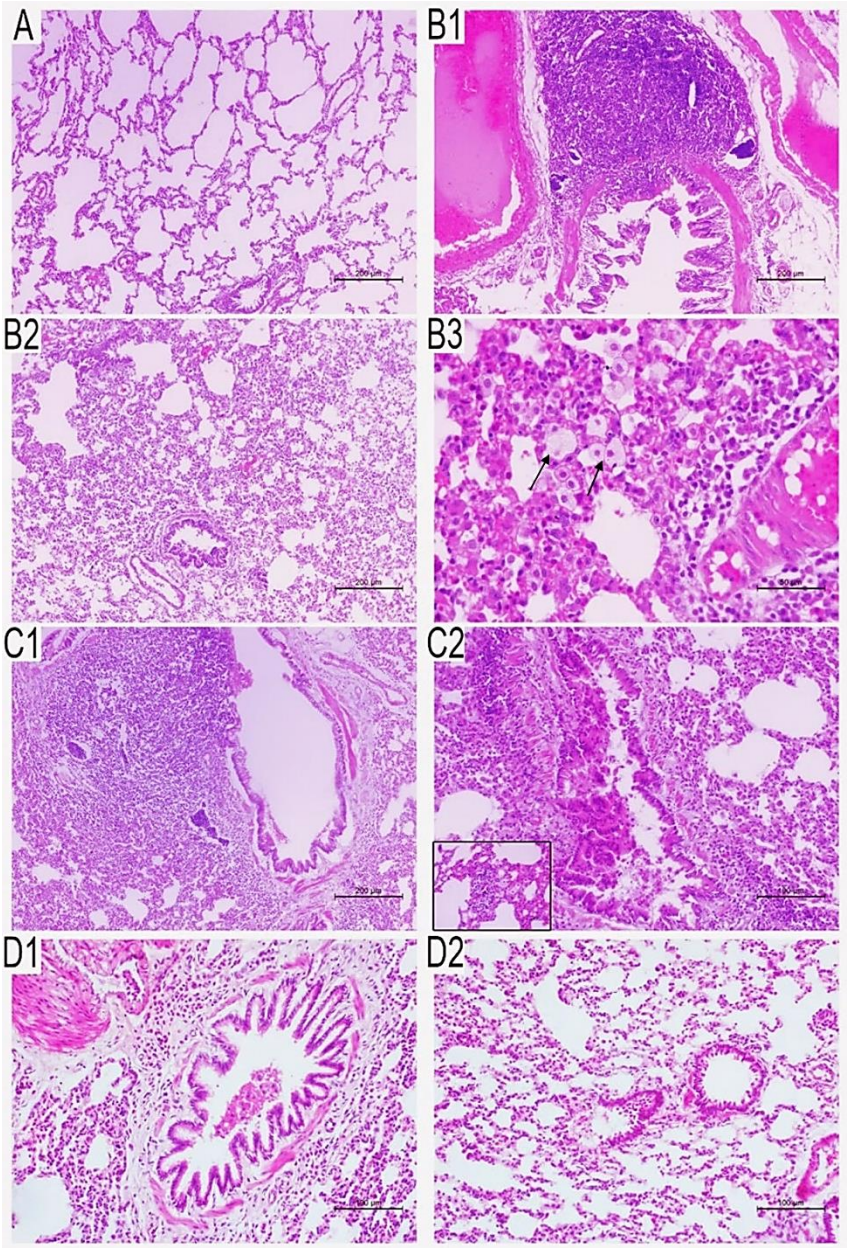

Fig. 8: Representative photomicrographs of rat lung sections stained with H&E. (A) control group, (B) MWCNT exposed group, (C) MWCNT+MSCs +Exosomes group, (D) MSCs +Exosomes treated group. Arrows and labels were explained in the main text. Scale bars, 200µm (A, B1, B2, C1), 50µm (B2), 100 µm (C2, D1, D2).

3.4 Area Percentages of Fibrosis Estimated with Masson's Trichrome stain

All measurements were tabulated in Table (2). Estimation of pulmonary fibrosis (the area percent of collagen fibers and collagen deposition in the lungs) was carried out, and the average area percentages of fibrosis in various groups were 8.47±3.34, 13.58± 4.37, 8.71±4.13, and 9.96±3.93 85 in the G1, G2, G3, and G4 groups, respectively.

Table 2: Morphometric comparison of the area percentages of fibrosis, hyperplasia of the lining epithelium and goblet cells hyperplasia integrated density area percentages in the lung in different groups (Mean ± SD).

Lung			
Group	Fibrosis %	bronchial Lining epithelium thickness	Goblet Cells Hyperplasia Integrated Density Area Percentages
G1	8.47±3.34	10.83 ±3.35	1.8029 ± 1.34344
G2	13.58 ± 4.37 ***	19.83 ± 7.23 ***	1.0301 ± 0.71482
G3	8.71 ± 4.13	14.13 ± 4.91 ***	0.6113 ± 0.48890 *
G4	9.96±3.93	14.52 ± 4.85 ***	1.1907 ± 1.02982

*Stars indicate significance in comparison with the control

Hue area measurements revealed varying degrees of fibrosis and hyperplasia across groups (Fig.9). The MWCNT-exposed group (G2) showed a significant increase in hue area (13.58 ± 4.38) compared to control (G1: 8.48±3.35, P<0.001), indicating MWCNT-induced brochial tissue changes. Co-treatment with MSC-exosomes (G3) significantly reduced hue area (8.72 ± 4.14) compared to G2 (P=0.013), suggesting therapeutic effects. The MSC-exosome-only group (G4) had a moderate hue area (9.97±3.93). No significant differences were found between G3 & G1 (P=1.000) or G4 & G1 (P=0.722), supporting the protective role of MSC-exosome therapy in restoring tissue conditions to near-normal levels (Fig. 10A).

3.5. Bronchial lining epithelium thickness

All measurements were tabulated in Table (2). The average of the lining epithelium of the bronchiole thickness or length in different groups was 10.83±3.35, 19.83± 7.23, 14.13±4.91, and 14.52±4.85 in the G1, G2, G3, and G4, respectively.

Bronchial epithelial length varied significantly among groups. The control group (G1) had the shortest mean length (10.84±3.35), indicating normal histology. MWCNT exposure (G2) resulted in marked epithelial hyperplasia (19.84±7.24, P<0.000 vs. G1). Co-treatment with MSC-exosomes (G3: 14.13±4.92) significantly reduced hyperplasia compared to G2 (P<0.000) and showed no significant difference from the MSC-exosome only group (G4: 14.53 ± 4.85, P=0.965). Both G3 and G4 had significantly higher values than G1 (P<0.000), suggesting mild hyperplasia in treated groups. These findings confirm that MWCNTs induce epithelial hyperplasia, while MSC-exosome therapy mitigates this effect, restoring epithelial thickness closer to normal (Fig. 10B).

3.6. Goblet Cells Hyperplasia Integrated Density Area Percentages

Assessment of goblet cell hyperplasia using PAS staining revealed notable variations among the experimental groups. The highest mean staining intensity was observed in the control group (G1: 1.8029 ± 1.34344), followed by the MSCs +Exosomes-only group (G4: 1.1907 ± 1.02982), the MWCNT-treated group (G2: 1.0301 ± 0.71482), and the lowest intensity in the MWCNT + MSCs +Exosomes group (G3: 0.6113 ± 0.48890). The marked reduction in PAS staining intensity in G3 suggests a mitigative effect of MSCs + Exosomes on MWCNT-induced goblet cell hyperplasia.

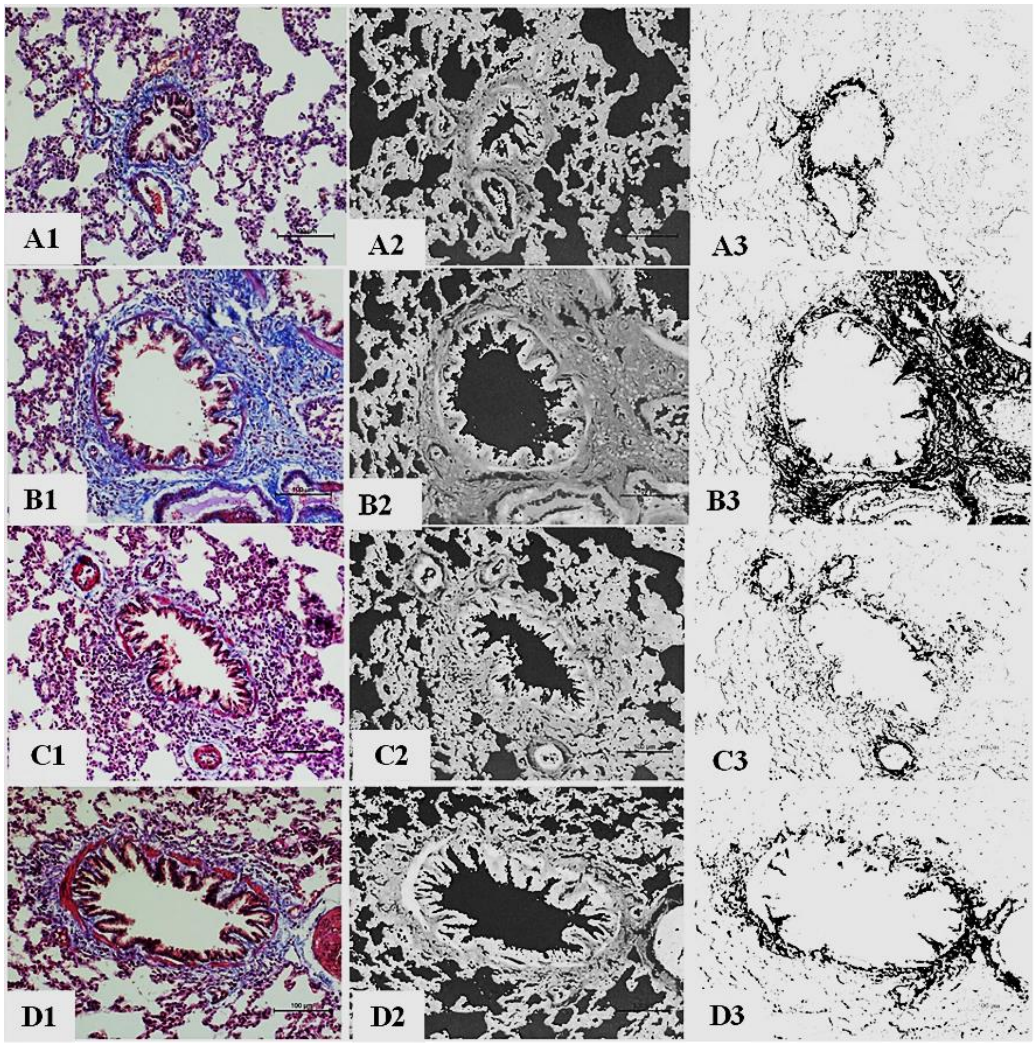

Fig. 9: Representative photomicrographs of rat lung sections stained with Masson's trichome (magnification 200x). Scale bars,100 µm: Lung sections showing different levels of histopathologic fibrosis proliferation around the bronchioles and blood vessels in different groups with blue color. (A-D), corresponding hue stacks used for measuring fibrosis area percentages. Area percentages of fibrosis were 4.516%, 23.544%, 6.033%, and 8.92%, respectively, in G1(A), G2 (B), G3 (C) and G4 (D).

Statistical analysis using Tukey's HSD post hoc test demonstrated a significant reduction in PAS intensity between the control (G1) and G3 (P=0.004). Although a reduction was observed between G1 and G2 (P=0.076), it did not reach statistical significance. Comparisons between G2 and G3 (P=0.675), and between G2 and G4 (P=0.380), showed no significant differences, indicating that the co-administration of MSCs+Exosomes with MWCNTs may be more effective in reducing goblet cell hyperplasia than either treatment alone (Figure 10C).

3.7. Oxidant and antioxidant biomarkers (Effect of MWCNTs and/or MSCs and exosomes on Lung Antioxidants and Oxidative Stress Markers)

In lung tissue homogenate, the MDA concentration was significantly elevated in the MWCNTs group (G2), compared to the control (G1) (P=0.000) and the MSCs associated with the exosomes group (G3) (P=0.003). However, the injection of MSCs associated with exosomes significantly reduced their concentration in group (G3) compared to the MWCNTs group (G2) (P=0.000). As for GSH levels, there were

no statistically significant differences between groups (P>0.05). Nevertheless, the MWCNTs group (G2) showed a slight numerical decrease compared to the Control (G1) and treatment groups (G3 and G4), suggesting a mild depletion trend in response to oxidative stress that did not reach significance. Total and protein thiols levels exhibited a consistent pattern across groups, with a marked and statistically significant depletion in G3 compared to all other groups. total thiols and protein thiols were significantly reduced in G3 relative to G1 (P=0.001), G2 (P=0.000), and G4 (P=0.000), indicating extensive oxidative consumption. (Fig.11).

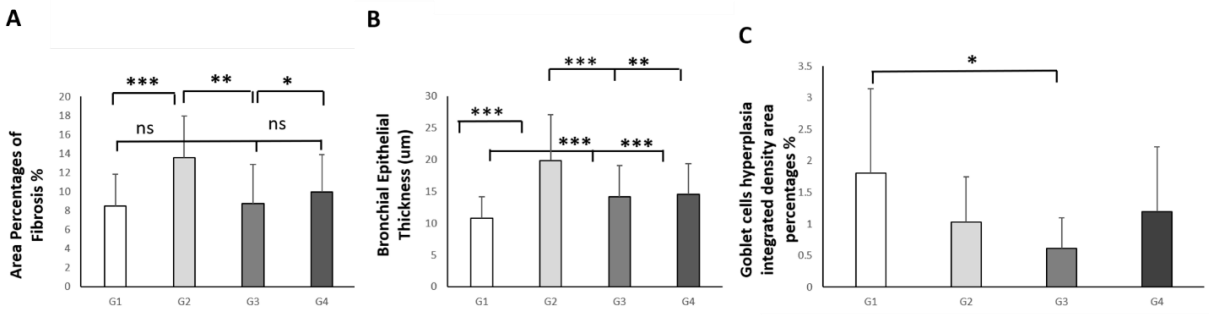

Fig. 10: Morphometric analysis of area percentages of fibrosis % (A), bronchial epithelial thickness (B), and goblet cells hyperplasia area percentages (C). (*P<0.05, **P<0.001, ***P<0.0001 and ns (Not significant). G1: control group; G2: MWCNTs intoxicated group; G3: MWCNTs intoxicated +MSCs and derived its Exosomes (toxic + treated group); G4: MSCs and its derived Exosomes treated group.

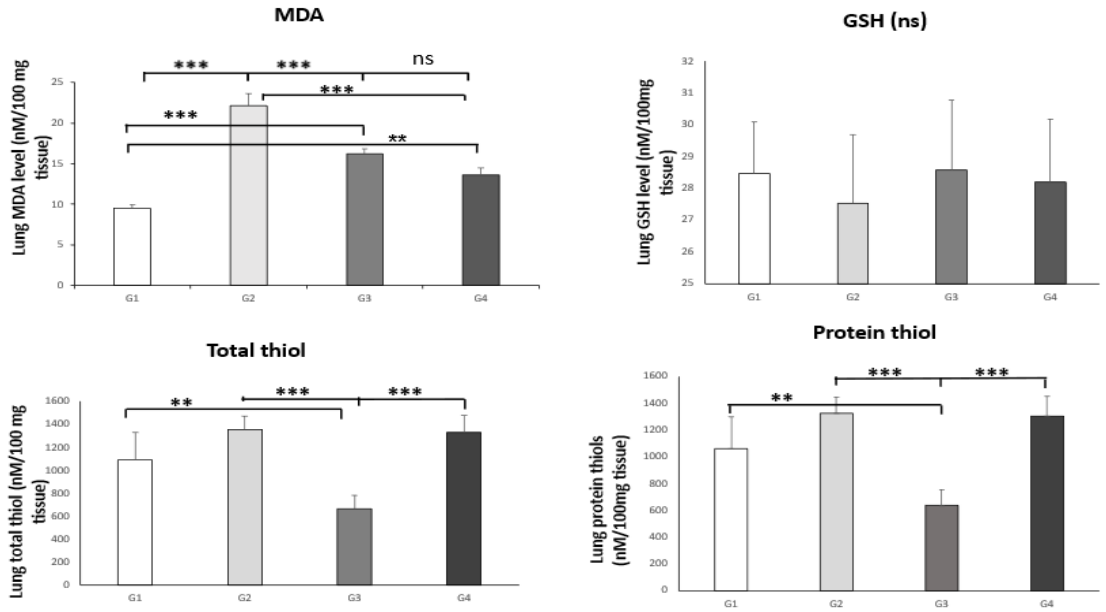

Fig. 11: Influence of MSCs associated with exosomes on ROS and MWCNTs-induced oxidative damage (as revealed by determination of MDA, GSH, total thiols, and protein thiols) in the lung of different experimental groups. Data were presented as mean ± SD, with significant differences at P<0.05. (*P<0.05, **P<0.001 and ***P<0.0001) and ns (Not significant) (n=6).

DISCUSSION

Carbon nanotubes find extensive use in industrial applications, despite growing healthcare concerns about their potential adverse effects on human health. The scientific literature has shown that CNTs produce cytotoxic, immunotoxic, neurotoxic, and genotoxic effects (Sallam *et al.,* 2022) and pulmonary toxicity effects (El-Gazzar *et al.,* 2018) in different tissues and cells. Research focuses predominantly

on identifying CNT-induced toxicity mechanisms, because the current medical care methods for prevention and treatment still lack effectiveness. The combination of tissue engineering with MSCs from different sources creates an advanced therapeutic approach, because MSCs possess both flexibility and easy access for medical use (Harting *et al.,* 2009; Hoogduijn *et al.,* 2013; Kabir *et al.,* 2020). MSC-derived exosomes function as intercellular communicators to perform therapeutic and diagnostic role finding applications mainly in cancer treatments and regenerative medicine processes, because they serve as effective delivery vehicles for targeted drugs and genetic materials (Hong *et al.,* 2019).

In the present investigation, we clearly demonstrated that the MWCNTs induced pulmonary toxic effects, as evidenced by decreased antioxidant status, increased oxidative stress markers, inflammatory reactions, in addition to significant lung tissue damage. These changes were marked by degeneration, necrosis, marked fibrosis (assessed via Masson's trichrome staining and morphometric analysis), hyperplastic changes in the lining epithelium, and goblet cell hyperplasia in the bronchiolar epithelium. This study used histological evaluation, coupled with morphometric analysis and ImageJ tools, to properly evaluate the toxicity level and the counteracting from MSCs and exosomes treatments.

With morphometric analysis of lung sections, Masson's trichrome staining revealed significantly increased collagen fiber deposition in the MWCNT group (G2) compared to both the control (G1) and treatment groups (G3). Consistent with these findings, previous reports showed that CNTs can cause lung inflammation and fibrosis by upregulating TNF-α production, leading to increased deposition of extracellular matrix (ECM) in alveolar septa, with lesions persisting post-exposure. (Muller *et al.,* 2005; Porter *et al.,* 2012; Dong *et al.,* 2014).

We found an increased number of free macrophages in the lungs of this group (G2). They are a major source of long, rigid CNT-associated reactive oxidants (Johnston *et al.,* 2010; Donaldson *et al.,* 2011). Macrophages serve an important role in immunological control, immune response, pulmonary host defense, and the clearing of injured cells and inhaled particles after lung injury (Lin *et al.,* 2019). In addition, there was a marked increase in the bronchial lining epithelium thickness in the MWCNTs group compared to other groups. This may be due to a response associated with foreign body reactions and chronic irritation from the deposition of MWCNTs (Umeda *et al.,* 2013). In their study, Umeda *et al.* (2013) also observed goblet cell hyperplasia in the nasal cavity and nasopharynx in rats exposed to 1 and 5 mg/m³ MWCNTs. This condition is distinguished by an increase in mucus production, which appears to facilitate the elimination of MWCNT deposits. Although the hyperplasia diminishes when the exposure disappears, the persistent mucus discharge shows the irritant and inflammatory effects of MWCNT fibers on the respiratory epithelium. This is consistent with our results that indicated increased goblet cell hyperplasia in the bronchial epithelium of the MWCNTs group.

Morphometric analysis showed that fibrosis was significantly reduced in the (G3) group compared to group (G2), suggesting a protective effect of the treatment. This reduction suggests an ameliorative effect of MSCs and exosomes. (MWCNTs) upregulate NLRP3, Caspase-1, and IL-1β, triggering inflammatory and fibrotic responses through NF-κB signaling and ROS release (He *et al.,* 2016; Zhong *et al.,* 2016; Keshavan *et al.,* 2021). In contrast, MSCs and their extracellular vesicles (hucMSC-EVs) counteract these effects by suppressing these inflammatory pathways and reducing fibrosis-related markers such as Collagen I, III, fibronectin, and α-SMA (El Agha *et al.,* 2017; Hou *et al.,* 2023b).

Wan *et al.* (2022) reported that bone marrow-derived MSC-EVs (BMMSC-EVs) reduce fibroblast proliferation by suppressing FZD6 expression via miR-29b-3p. Similarly, Zhou *et al.* (2022) found that miR-186 in BMMSC-EVs downregulates SOX4 and DKK1, thereby preventing fibroblast activation and alleviating idiopathic pulmonary fibrosis (IPF). In addition to targeting fibroblasts, MSC-EVs modulate inflammation, a critical factor in fibrosis.

The histopathological and morphometric analysis revealed a significant decrease in goblet cell hyperplasia and epithelial thickness in the G3 group compared to G2, confirming the ameliorative effects of MSCs and exosomes. Previous studies have corroborated these findings, demonstrating that treatment with MSCs and exosomes markedly reduces bronchial epithelium thickness and goblet cell hyperplasia in lung tissues. align with earlier studies, such as Lee *et al.* (2011), who demonstrated that MSCs alleviate airway remodeling including goblet cell hyperplasia and collagen deposition. Similarly, Nemeth *et al.* (2010) reported reduced Th2 inflammation following MSC therapy in allergic airway disease.

Increased ROS levels were also observed in the lungs of MWCNT-treated rats, consistent with earlier reports that ROS are by-products of oxygen metabolism and central to cell signalling, but harmful at excessive levels (Muthu *et al.,* 2013). MWCNT exposure raised MDA levels, indicating lipid peroxidation and oxidative tissue damage, while decreasing glutathione (GSH), an essential antioxidant (Elmoslemany *et al.,* 2021; Mohamed *et al.,* 2021). Elevated MDA levels and reduced GSH were associated with disrupted redox balance, damaging the phospholipid-rich membranes (El-Magd *et al.,* 2016; Abdelhady *et al.,* 2017; Mohamed *et al.,* 2019). Similar effects have been reported in the brain (Visalli *et al.,* 2017; Adedara *et al.,* 2020), kidneys (Abu Gazia and El-Magd, 2018), and spleen (Sallam *et al.,* 2022).

In contrast, total thiols and protein thiols levels increased in the MWCNTs group. According to Pichardo *et al.* (2012), who investigated that oxidative stress is indicated by decreased endogenous antioxidant levels, but oxidative stress can be interpreted as a reaction to elevated amounts of the same antioxidant. For example, it was demonstrated that 24-hour exposure to CNT in Caco-2 cells enhanced catalase and SOD activity, possibly as a compensatory defines and decreased GSH levels.

MSCs are known to withstand oxidative stress and can mitigate ROS-related tissue injury in various disease models (Stavely and Nurgali, 2020). In the present study, MSCs and MSC-exosomes significantly reduced MDA and increased GSH levels in the treated group compared to the untreated MWCNT group. Their antioxidant effects are attributed to their protein and miRNA content. Wang et al. (2020) reported that MSC-EVs improve calcium influx, decrease pro-inflammatory molecules, and reduce ROS. Additionally, Zheng et al. (2021) demonstrated that exosomes, especially those enriched with miR-22-3p, increased SOD and GSH activity while decreasing MDA in alveolar macrophages (NR8383 cells).

CONCLUSION

In conclusion, this study demonstrated that MSCs and exosomes significantly alleviated the toxic effects of MWCNTs in albino rats by reducing lung fibrosis, oxidative stress, epithelial hyperplasia, and goblet cell proliferation. Histological and morphometric analyses using H&E and Masson's trichrome stains, along with ImageJ software, provided precise quantification of tissue alterations, offering strong evidence for the therapeutic potential of MSCs and their exosomes in managing MWCNTs-induced lung damage.

List of abbreviations

MWCNTs	Multi-walled carbon nanotubes
MSCs	Mesenchymal stem cells
MDA	Malondialdehyde
GSH	Glutathione
WSI	Whole slide imaging
NIH	National Institutes of Health
CNTs	Carbon nanotubes
SWCNTs	Single-walled carbon nanotubes
IL-10	Interleukin-10
TNF	Tumor Necrosis Factor
(MSC-Exos)	Exosomes derived from MSCs
EPRI	Egyptian Petroleum Research Institute
SEM	Scanning electron microscopy
TEM	transmission electron microscopy
HRTEM	High-resolution transmission electron microscopy
FESEM	field emission scanning electron microscopy
EDX	Energy-dispersive X-ray
XRD	X-ray diffraction
WJ-MSCs	Mesenchymal stem cells from Wharton Jelly
DMEM	Dulbecco's Modified Eagle's Medium
FBS	Fetal bovine serum
ISCT	International Society for Cellular Therapy
CD	Cluster of Differentiation
hUC-MSC	Human umbilical cord mesenchymal stem cells
PE	Phycoerythrin
FITC	Fluorescein isothiocyanate
BSU-IACUC	Institutional Animal Care and Use Committee of Beni-Suef University
IP	Intraperitoneal
PBS	phosphate-buffered saline
H&E	Hematoxylin and eosin stain
PAS	Periodic acid–Schiff
hucMSC-EVs	Human umbilical MSCs and their extracellular vesicles
IPF	Idiopathic pulmonary fibrosis
Th2	T helper cell type 2
ROS	Reactive Oxygen Species
SOD	Superoxide dismutase
IL-1β	Interleukin-1 beta
NF-κB	Nuclear Factor kappa-light-chain-enhancer of activated B cells
NLRP3	Nucleotide-binding oligomerization domain-like receptor, pyrin domain-containing 3 inflammasome pathways
α-SMA	Alpha-smooth muscle actin
FZD6	Frizzled Class Receptor 6
miR-29b-3p	MicroRNA-29b-3p
SOX4	SRY-Box Transcription Factor 4
DKK1	Dickkopf WNT Signaling Pathway Inhibitor 1

REFERENCES

Abdelhady, D.; El-Abasy, M.; Abou-Asa, S.; Elbialy, Z.; Shukry, M.; Hussein, A.; Saleh, A. and El-Magd, M. (2017): The ameliorative effect of Aspergillus awamori on aflatoxin B1-induced hepatic damage in rabbits. World Mycotoxin Journal, 10(4), 363–373. https://doi.org/10.3920/WMJ2017.2188

Abu Gazia, M. and El-Magd, M.A. (2018): Effect of pristine and functionalized multiwalled carbon nanotubes on rat renal cortex. Acta Histochemica, 121(2), 207–217.

https://doi.org/10.1016/j.acthis.2018.01.002

Abu Gazia, M. and El-Magd, M.A. (2019): Effect of pristine and functionalized multiwalled carbon nanotubes on rat renal cortex. *Acta Histochemica*, *121*(2), 207–217. https://doi.org/10.1016/j.acthis.2018.12.005

Abu Gazia, M. and El-Magd, M.A. (2019): Effect of pristine and functionalized multiwalled carbon nanotubes on rat renal cortex. *Acta Histochemica*, *121*(2), 207–217. https://doi.org/10.1016/j.acthis.2018.12.005

Adedara, I.A.; Awogbindin, I.O.; Owoeye, O.; Maduako, I.C.; Ajeleti, A.O.; Owumi, S.E.; Patlolla, A.K. and Farombi, E.O. (2020): Kolaviron via anti-inflammatory and redox regulatory mechanisms abates multi-walled carbon nanotubes-induced neurobehavioral deficits in rats. Psychopharmacology, 237(4), 1027–1040. https://doi.org/10.1007/s00213-020-05455-6

Aeffner, F.; Zarella, M.D.; Buchbinder, N.; Bui, M.M.; Goodman, M.R.; Hartman, D.J. and Parwani, A.V. (2019): Introduction to digital image analysis in whole-slide imaging: a white paper from the Digital Pathology Association. *Journal of Pathology Informatics*, 10, 9. https://doi.org/10.4103/jpi.jpi_46_18 ResearchGate+1PubMed+1

Aggarwal, S. and Pittenger, M.F. (2005): Human mesenchymal stem cells modulate allogeneic immune cell responses. *Blood*, *105*(4), 1815–1822. https://doi.org/10.1182/blood-2004-04-1559

Aijaz, A.; Li, M.; Smith, D.; Khong, D.; LeBlon, C.; Fenton, O.S.; Olabisi, R.M.; Libutti, S.; Tischfield, J.; Maus, M.V.; Deans, R.; Barcia, R.N.; Anderson, D.G.; Ritz, J.; Preti, R. and Parekkadan, B. (2018): Biomanufacturing for Clinically Advanced Cell Therapies.

Ali, D.; Falodah, F.A.; Almutairi, B.; Alkahtani, S. and Alarifi, S. (2020): Assessment of DNA damage and oxidative stress in juvenile *Channa punctatus* (Bloch) after exposure to multi-walled carbon nanotubes. *Environmental Toxicology*, 35(3), 359–367. https://doi.org/10.1002/tox.22871

Almaeen, AH.; Saad-Eldien, HM. And Gabr, H. (2025): INF-γ/TGF-β1-primed umbilical cord mesenchymal stem cells boost the T-lymphocytes activity: Modulation of CD25 expression and IL-6 secretion. Int J Immunopathol Pharmacol. 2025 Jan-Dec;39:3946320251315007.doi: 10.1177/03946320251315007. PMID: 39921228; PMCID: PMC11806471

Alosime, E.M. (2023): A review on surface functionalization of carbon nanotubes: methods and applications. *Discover Nano*, *18*(1). https://doi.org/10.1186/s11671-023-03789-6

Bancroft, J.D. and Layton, C. (2019): The hematoxylins and eosin, p. 126–138. *In* S.K. Suvarna, C. Layton, and J.D. Bancroft (eds.), Bancroft's Theory and Practice of Histological Techniques, 8th ed. Elsevier, Philadelphia, USA.

Cifuentes-Rius, A.; Boase, N.R.B.; Font, I.; Coronas, N.; Ramos-Perez, V.; Thurecht, K.J. and Borrós, S. (2017): In Vivo Fate of Carbon Nanotubes with Different Physicochemical Properties for Gene Delivery Applications. ACS Appl. Mater. Interfaces 2017, 9, 11461–11471. [CrossRef] [PubMed]

Czarny, B.; Georgin, D.; Berthon, F.; Plastow, G.; Pinault, M.; Patriarche, G.; Thuleau, A.; L'Hermite, M.M.; Taran, F. and Dive, V. (2014): Carbon nanotube translocation to distant organs after pulmonary exposure: insights from in situ 14C-

radiolabeling and tissue radioimaging. ACS Nano, 8(6), 5715–5724. https://doi.org/10.1021/nn5011914

Deroulers, C.; Ameisen, D.; Badoual, M.; Marin, C. and Pinel, P. (2013): Analyzing huge pathology images with open source software. *Diagnostic Pathology*, 8, 92. https://doi.org/10.1186/1746-1596-8-92BioMed Central+1ResearchGate+1

Donaldson, K.; Murphy, F.; Schinwald, A.; Duffin, R. and Poland, CA. (2011): Identifying the pulmonary hazard of high aspect ratio nanopar ticles to enable their safety-by-design. Nanomedicine (Lond) 6(1):143–156. https://doi.org/10.2217/nnm.10.139

Dong, J.; Porter, DW.; Batteli, LA.; Wolfarth, MG.; Richardson, DL. and Ma, Q. (2015): Pathologic and molecular profiling of rapid-onset fibrosis and inflammation induced by multi-walled carbon nanotubes. Arch Toxicol (2015) 89(4):621–33. doi: 10.1007/s00204-014-1428-y

Ebrahim, N.; Ahmed, I.; Hussien, N.; Dessouky, A.; Farid, A.; Elshazly, A.; Mostafa, O.; Gazzar, W.; Sorour, S.; Seleem, Y.; Hussein, A. and Sabry, D. (2018): Mesenchymal stem cell-derived exosomes ameliorated diabetic nephropathy by autophagy induction through the mTOR signaling pathway. *Cells*, *7*(12), 226. https://doi.org/10.3390/cells7120226

El Agha, E.; Kramann, R.; Schneider, RK.; Li, X.; Seeger, W. and Humphreys, BD, et al. Mesenchymal stem cells in fibrotic disease. Cell Stem Cell. 2017;21(2):166–77.

El-Gazzar, A.M.; Abdelgied, M.; Alexander, D.B.; Alexander, W.T.; Numano, T.; Iigo, M.; Naiki, A.; Takahashi, S.; Takase, H.; Hirose, A.; Kannno, J.; Elokle, O.S.; Nazem, A.M. and Tsuda, H. (2018): Comparative pulmonary toxicity of a DWCNT and MWCNT-7 in rats. *Archives of Toxicology*, *93*(1), 49–59. https://doi.org/10.1007/s00204-018-2336-3

Ellman, G.L. (1959): Tissue sulfhydryl groups. Archives of Biochemistrya and Biophysics, 82(1), 70–77. https://doi.org/10.1016/0003-9861(59)90090-6.

El-Magd, M.A.; Kahilo, K.A.; Nasr, N.E.; Kamal, T.; Shukry, M. and Saleh, A.A. (2017): A potential mechanism associated with lead-induced testicular toxicity in rats. Andrologia, 49(9), e12750. https://doi.org/10.1111/and.12750

Elmoslemany, A.M.; El-Magd, M.A.; Ghamry, H.I.; Alshahrani, M.Y.; Zidan, N.S. and Zedan, A.M.G. (2021): Avocado seeds relieve oxidative stress-dependent nephrotoxicity but enhance immunosuppression induced by cyclosporine in rats. Antioxidants, 10(8), 1194. https://doi.org/10.3390/antiox10081194

El-Nahass, E.; Moselhy, W.A. and Hassan, N.E.Y. (2017): Forensic Image Analyses of Skin and Underlying Muscles as a Tool for Postmortem Interval Delimitation. *American Journal of Forensic Medicine & Pathology*, *38*(2), 131–138. https://doi.org/10.1097/paf.0000000000000301

Flotte, T.J.; Springer, T.A. and Thorbecke, G.J. (1989): Immunohistochemical localization of lymphocyte function-associated antigen-1 in human tissues. *The American Journal of Pathology*, 134(1), 1–6.

Friedenstein, A.J.; Piatetzky-Shapiro, I.I. and Petrakova, K.V. (1966): Osteogenesis in transplants of bone marrow cells. Development, 16(3), 381–390. https://doi.org/10.1242/dev.16.3.381

G. Visalli; M. Curr` o; D. Iannazzo; A. Pistone; M. Pruiti Ciarello; G. Acri; B. Testagrossa; M.P. Bertuccio and R. Squeri (2017): A. Di Pietro, In vitro assessment of neurotoxicity and

neuroinflammation of homemade MWCNTs, Environ. Toxicol. Pharmacol. 56 (2017) 121–128. (Visalli et al., 2017).

Girish, V. and Vijayalakshmi, A. (2004): Affordable image analysis using NIH Image/ImageJ. *Indian Journal of Cancer*, 41(1), 47. https://doi.org/10.4103/0019-509X.11666

Griffin, J. and Treanor, D. (2017): Digital pathology in clinical use: where are we now and what is holding us back? *Histopathology*, 70(1), 134–145. https://doi.org/10.1111/his.12993 ResearchGate+2Wiley Online Library+2PubMed+2

Gupta, S.; Rawat, S. and Arora, V. et al. (2018): An improvised one-step sucrose cushion ultracentrifugation method for exosome isolation from culture supernatants of mesenchymal stem cells. Stem Cell Research & Therapy 9:1–11. https://doi.org/10.1186/s13287-018-0923-0.

Hamilton, P.W.; Bankhead, P.; Wang, Y.; Hutchinson, R.; Kieran, D.; McArt, D.G. and James, J.A. (2014): Digital pathology and image analysis in tissue biomarker research. *Methods*, 70(1), 59–73. https://doi.org/10.1016/j.ymeth.2014.06.016 PubMed+2ScienceDirect+2ScienceDirect+2

Harting, MT.; Jimenez, F. and Xue, H. et al. (2009): Intravenous mesenchymal stem cell therapy for traumatic brain injury. J Neurosurg. 2009;110 (6):1189–1197. doi:10.3171/2008.9.JNS08158

He, Y.; Hara, H. and Núñez, G. (2016): Mechanism and regulation of NLRP3 inflammasome activation. Trends in Biochemical Sciences, 41(12), 1012–1021. https://doi.org/10.1016/j.tibs.2016.09.002

Hong, M.K.H.; Lee, S.E. and Kim, Y.J. (2020): Role of artificial intelligence in digital pathology for gynecological cancers. *Journal of Pathology and Translational Medicine*, 54(2), 105–113. https://doi.org/10.4132/jptm.2019.12.24PMC

Hong, P.; Yang, H.; Wu, Y.; Li, K. and Tang, Z. (2019): The functions and clinical application potential of exosomes derived from adipose mesenchymal stem cells: a comprehensive review. *Stem Cell Research & Therapy*, *10*(1). https://doi.org/10.1186/s13287-019-1358-y

Hoogduijn, MJ.; Roemeling-van Rhijn, M. and Engela, AU. et al. (2013): Mesenchymal stem cells induce an inflammatory response after intra venous infusion. Stem Cells Dev. 2013;22(21):2825–2835. doi:10.1089/scd.2013.0193

Hou, L.; Zhu, Z.; Jiang, F.; Zhao, J.; Jia, Q.; Jiang, Q.; Wang, H.; Xue, W.; Wang, Y. and Tian, L. (2023b): Human umbilical cord mesenchymal stem cell-derived extracellular vesicles alleviated silica induced lung inflammation and fibrosis in mice via circPWWP2A/miR-223–3p/NLRP3 axis. *Ecotoxicology and Environmental Safety*, *251*, 114537. https://doi.org/10.1016/j.ecoenv.2023.114537

Jacobsen, N.R.; Møller, P.; Clausen, P.A.; Saber, A.T.; Micheletti, C.; Jensen, K.A.; Wallin, H. and Vogel, U. (2016): Biodistribution of carbon nanotubes in animal models. Basic & Clinical Pharmacology & Toxicology, 119(2), 143–151. https://doi.org/10.1111/bcpt.12705

Jahn, S.W.; Plass, M. and Moinfar, F. (2020): Digital pathology: advantages, limitations and emerging perspectives. *Journal of Clinical Medicine*, 9(11), 3697. https://doi.org/10.3390/jcm9113697 MDPI+1PubMed+1

Jensen, C.; Engberg, R.; Jakobsen, K.; Skibsted, L. and Bertelsen, G. (1997):

Influence of the oxidative quality of dietary oil on broiler meat storage stability. *Meat Science, 47*(3–4), 211–222. https://doi.org/10.1016/S0309-1740(97)00052-1

Jiang, Y.; Jahagirdar, BN. and Reinhardt, RL. et al. (2202): Pluripotency of mesench ymal stem cells derived from adult marrow. Nature. 2002;418 (6893):41–49. doi:10.1038/nature00870

Johnston, HJ.; Hutchison, GR. and Christensen, FM. et al (2010): A critical review of the biological mechanisms underlying the in vivo and in vitro toxicity of carbon nanotubes: the contribution of physico chemical characteristics. Nanotoxicology 4(2):207–246. https :// doi.org/10.3109/17435390903569639

*Kabir, W.; Di Bella, C.; Jo, I.; Gould, D. and Choong, P.F.M. (2020):*Human stem cell based tissue engineering for in vivo cartilage repair: a systematic review. Tissue Eng Part B Rev. 2020. doi: 10.1089/ten.TEB.2020.0155.

Keshavan, S.; Gupta, G.; Martin, S. and Fadeel, B. (2021): Multi-walled carbon nanotubes trigger lysosome-dependent cell death (pyroptosis) in macrophages but not in neutrophils. Nanotoxicology, 15(9), 1125–1150. https://doi.org/10.1080/17435390.2021.1988171

Kobler, C.; Poulsen, S.S.; Saber, A.T.; Jacobsen, N.R.; Wallin, H.; Yauk, C.L.; Halappanavar, S.; Vogel, U.; Qvortrup, K. and Mølhave, K. (2015): Time-dependent subcellular distribution and effects of carbon nanotubes in lungs of mice. PLoS ONE, 10(4), e0116481. https://doi.org/10.1371/journal.pone.0116481

Kopen, G.C.; Prockop, D.J. and Phinney, D.G. (1999): Marrow stromal cells migrate throughout forebrain and cerebellum, and they differentiate into astrocytes after injection into neonatal mouse brains. *Proceedings of the National Academy of Sciences*, *96*(19), 10711–10716. https://doi.org/10.1073/pnas.96.19.10711

Lee, SH.; Jang, AS.; Kwon, JH.; Park, SK.; Won, JH. and Park, CS. (2011): Mesenchymal stem cell transfer suppress airway remodeling in a toluene diisocyanate-induced murine asthma model. Allergy Asthma Immunol Res 2011;3:205–11 [Pubmed: 21738887].

Lin, C.R. et al. (2019): S100A8 protects human primary alveolar type II cells against injury and emphysema. Am. J. Respir. Cell Mol. Biol. 60, 299–307.

Liu, Y. and Pantanowitz, L. (2019): Digital pathology: review of current opportunities and challenges for oral pathologists. *Journal of Oral Pathology & Medicine*, 48(4), 263–269. https://doi.org/10.1111/jop.12825 Rutgers University+2PubMed+2Wiley Online Library+2

Ma, M.; Li, B.; Zhang, M.; Zhou, L.; Yang, F.; Ma, F.; Shao, H.; Li, Q.; Li, X. and Zhang, X. (2020): Therapeutic effects of mesenchymal stem cell-derived exosomes on retinal detachment. Experimental Eye Research, 191, 107899. https://doi.org/10.1016/j.exer.2019.107899

Madabhushi, A. and Lee, G. (2016): Image analysis and machine learning in digital pathology: challenges and opportunities. *Medical Image Analysis*, 33, 170–175. https://doi.org/10.1016/j.media.2016.06.037PubMed+1ResearchGate+1

Madannejad, R.; Shoaie, N.; Jahanpeyma, F.; Darvishi, M.H.; Azimzadeh, M. and Javadi, H. (2019): Toxicity of carbon-based nanomaterials: Reviewing recent reports in medical and biological systems. *Chemico-Biological Interactions*, *307*, 206–222.

https://doi.org/10.1016/j.cbi.2019.04.036

Madannejad, R.; Shoaie, N.; Jahanpeyma, F.; Darvishi, M.H.; Azimzadeh, M. and Javadi, H. (2019): Toxicity of carbon-based nanomaterials: Reviewing recent reports in medical and biological systems. *Chemico-Biological Interactions*, *307*, 206–222. https://doi.org/10.1016/j.cbi.2019.04.036

Mercer, R.R.; Hubbs, A.F.; Scabilloni, J.F.; Wang, L.; Battelli, L.A.; Friend, S.; Castranova, V. and Porter, D.W. (2011): Pulmonary fibrotic response to aspiration of multi-walled carbon nanotubes. Particle and Fibre Toxicology, 8(1), 21. https://doi.org/10.1186/1743-8977-8-21

Miot, H.A.; Brianezi, G. and Marques, M.E.A. (2007): Morphometric analysis of collagen in keloids, hypertrophic scars, and normal skin. *Anais Brasileiros de Dermatologia*, 82(5), 511–515. https://doi.org/10.1590/S0365-05962007000500005

Mohamed, A.E.; El-Magd, M.A.; El-Said, K.S.; El-Sharnouby, M.; Tousson, E.M. and Salama, A.F. (2021): Potential therapeutic effect of thymoquinone and/or bee pollen on fluvastatin-induced hepatitis in rats. Scientific Reports, 11(1), 15688. https://doi.org/10.1038/s41598-021-95342-7

Mohamed, Y.; Basyony, M.A.; El-Desouki, N.I.; Abdo, W.S. and El-Magd, M.A. (2019): The potential therapeutic effect for melatonin and mesenchymal stem cells on hepatocellular carcinoma. BioMedicine, 9(4), 23–29. https://doi.org/10.37796/2211-8039.1004

Muller, J.; Huaux, F.; Moreau, N.; Misson, P.; Heilier, J.; Delos, M.; Arras, M.; Fonseca, A.; Nagy, J.B. and Lison, D. (2005b): Respiratory toxicity of multi-wall carbon nanotubes. *Toxicology and Applied Pharmacology*, *207*(3), 221–231. https://doi.org/10.1016/j.taap.2005.01.008

Muthu, M.S.; Abdulla, A. and Pandey, B.L. (2013): Major toxicities of carbon nanotubes induced by reactive oxygen species: should we worry about the effects on the lungs, liver and normal cells?. *Nanomedicine*, *8*(6), 863-866.

Nam, S.; Chong, Y.; Jung, C.K.; Kwak, T.Y.; Lee, J.Y.; Park, J. and Kim, S. (2020): Introduction to digital pathology and computer-aided pathology. *Journal of Pathology and Translational Medicine*, 54(2), 125–134. https://doi.org/10.4132/jptm.2019.12.23PMC

Nast, C.C.; Lemley, K.V.; Bagnasco, S.M. and Hodgin, J.B. (2015): Morphometry predicts early GFR change in primary proteinuric glomerulopathies: a longitudinal cohort study using generalized estimating equations. *PLOS ONE*, 10(6), e0130913. https://doi.org/10.1371/journal.pone.0130913PMC

Nemeth, K.; Keane-Myers, A.; Brown, JM.; Metcalfe, DD.; Gorham, JD. and Bundoc, VG. et al. (2010): Bone marrow stromal cells use TGF-β to suppress allergic responses in a mouse model of ragweed-induced asthma. Proc Natl Acad Sci U S A 2010;107:5652–7 [Pubmed: 202314466].

Öner, D.; Ghosh, M.; Bové, H.; Moisse, M.; Boeckx, B.; Duca, R.C.; Poels, K.; Luyts, K.; Putzeys, E. and Van Landuydt, K. (2018): Differences in MWCNT- and SWCNT-induced DNA methylation alterations in association with the nuclear deposition. Particle and Fibre Toxicology, 15(1), 1–19. https://doi.org/10.1186/s12989-018-0244-6 oxidative quality of dietary oil

on broiler meat storage stability, Meat Science 47

Pallua, J.D.; Brunner, A.; Zelger, B. and Schirmer, M. (2020): The future of pathology is digital. *Pathology-Research and Practice*, 216(11), 153040. https://doi.org/10.1016/j.prp.2020.153040ScienceDirect+1PubMed+1

Petersen, B.E.; Bowen, W.C.; Patrene, K.D.; Mars, W.M.; Sullivan, A.K.; Murase, N.; Boggs, S.S.; Greenberger, J.S. and Goff, J.P. (1999): Bone Marrow as a potential source of hepatic oval cells. *Science*, *284*(5417), 1168–1170. https://doi.org/10.1126/science.284.5417.1168

Pichardo, S.; Gutierrez-Praena, D.; Puerto, M.; Sanchez, E.; Grilo, A.; Camean, AM. and Jos, A. (2012): Oxidative stress responses to car boxylic acid functionalized single wall carbon nanotubes on the human intestinal cell line Caco-2. Toxicol In Vitro 26:672–677

Pittenger, M.F.; Mackay, A.M.; Beck, S.C.; Jaiswal, R.K.; Douglas, R.; Mosca, J.D.; Moorman, M.A.; Simonetti, D.W.; Craig, S. and Marshak, D.R. (1999): Multilineage potential of adult human mesenchymal stem cells. Science, 284(5411), 143–147. https://doi.org/10.1126/science.284.5411.143

Porter, DW.; Hubbs, AF.; Chen, BT.; McKinney, W.; Mercer, RR. and Wolfarth, MG, et al. (2012): Acute pulmonary dose-responses to inhaled multi-walled carbon nanotubes. Nanotoxicology (2013) 7(7):1179–94. doi: 10.3109/17435390.2012.719649

Poulsen, S.S.; Jackson, P.; Kling, K.; Knudsen, K.B.; Skaug, V.; Kyjovska, Z.O.; Thomsen, B.L.; Clausen, P.A.; Atluri, R.; Berthing, T.; Bengtson, S.; Wolff, H.; Jensen, K.A.; Wallin, H. and Vogel, U. (2016): Multi-walled carbon nanotube physicochemical properties predict pulmonary inflammation and genotoxicity. Nanotoxicology, 10(9), 1263–1275. https://doi.org/10.3109/17435390.2016.1146356

Raffaghello, L.; Bianchi, G.; Bertolotto, M.; Montecucco, F.; Busca, A.; Dallegri, F.; Ottonello, L. and Pistoia, V. (2007): Human mesenchymal stem cells inhibit neutrophil apoptosis: A model for neutrophil preservation in the bone marrow niche. *Stem Cells*, *26*(1), 151–162. https://doi.org/10.1634/stemcells.2007-0416

Royce, S.G.; Sedjahtera, A.; Samuel, C.S. and Tang, M.L.K. (2012): Combination therapy with relaxin and methylprednisolone augments the effects of either treatment alone in inhibiting subepithelial fibrosis in an experimental model of allergic airways disease. *Clinical Science*, *124*(1), 41–51. https://doi.org/10.1042/cs20120024

Sakamoto, Y.; Hojo, M.; Kosugi, Y.; Watanabe, K.; Hirose, A.; Inomata, A.; Suzuki, T. and Nakae, D. (2018): Comparative study for carcinogenicity of 7 different multi-wall carbon nanotubes with different physicochemical characteristics by a single intraperitoneal injection in male Fischer 344 rats. *The Journal of Toxicological Sciences*, *43*(10), 587–600. https://doi.org/10.2131/jts.43.587

Sallam, A.A.; Ahmed, M.M.; El-Magd, M.A.; Magdy, A.; Ghamry, H.I.; Alshahrani, M.Y. and Abou El-Fotoh, M.F. (2022): Quercetin-ameliorated, multi-walled carbon nanotubes-induced immunotoxic, inflammatory, and oxidative effects in mice. Molecules, 27(7), 2117. https://doi.org/10.3390/molecules27072117

Sallam, A.A.; El-Magd, M.A.; Ahmed, M.M.; Ghamry, H.I.; Alshahrani, M.Y.; Hegazy, R.A.; Magdy, A. and El-Fotoh, M.F.A. (2022): Quercetin alleviated multi-walled carbon

nanotubes-induced neurotoxicity in mice through inhibition of oxidation, inflammation, and pyroptosis. *Biomedicine & Pharmacotherapy*, *151*, 113160. https://doi.org/10.1016/j.biopha.2022.113160

Sedlakand, J. and Lindsay, R.H. (1968): Estimation of total, protein-bound, and non- protein sulfhydryl groups in tissue with Ellman's reagent. Analytical Biochemistry, 25 (1), 192–205. https://doi.org/10.1016/0003-2697(68)90092-4.

Talkar, S.; Dhoble, S.; Majumdar, A. and Patravale, V. (2018): Transmucosal nanoparticles: Toxicological overview. *Advances in Experimental Medicine and Biology*, *1048*, 37–57. https://doi.org/10.1007/978-3-319-72041-8_3/COVER

Umeda, Y.; Kasai, T.; Saito, M.; Kondo, H.; Toya, T.; Aiso, S.; Okuda, H.; Nishizawa, T. and Fukushima, S. (2013): Two-week Toxicity of Multi-walled Carbon Nanotubes by Whole-body Inhalation Exposure in Rats. *Journal of Toxicologic Pathology*, *26*(2), 131–140. https://doi.org/10.1293/tox.26.131

Visalli, G.; Facciolà, A.; Currò, M.; Laganà, P.; La Fauci, V.; Iannazzo, D.; Pistone, A. and Di Pietro, A. (2019): Mitochondrial Impairment Induced by Sub-Chronic Exposure to Multi-Walled Carbon Nanotubes. *International Journal of Environmental Research and Public Health*, *16*(5), 792. https://doi.org/10.3390/ijerph16050792

Wang, T.; Jian, Z.; Baskys, A.; Yang, J.; Li, J. and Guo, H. et al. (2020): MSC-derived exosomes protect against oxidative stress-induced skin injury via adaptive regulation of the NRF2 defense system. Biomaterials (2020) 257:120264. doi: 10.1016/ j. biomaterials.2020.120264

Wang, T.; Jian, Z.; Baskys, A.; Yang, J.; Li, J. and Guo, H. et al. (2020): MSC-derived exosomes protect against oxidative stress-induced skin injury via adaptive regulation of the NRF2 defense system. Biomaterials (2020) 257:120264. doi: 10.1016/ j.biomaterials.2020.120264

Wang, J.; Li, K.; Hao, D.; Li, X.; Zhu, Y.; Yu, H. and Chen, H. (2024): Pulmonary fibrosis: pathogenesis and therapeutic strategies. *MedComm*, *5*(10). https://doi.org/10.1002/mco2.744

Witkowska, M.; Florek, E. and Mrówczyński, R. (2022): Assessment of Pristine Carbon Nanotubes Toxicity in Rodent Models. International Journal of Molecular Sciences, 23(23), 15343. https://doi.org/10.3390/ijms232315343

Wynn, T.A. (2011): Integrating mechanisms of pulmonary fibrosis. *Journal of Experimental Medicine*, *208*(7), 1339–1350. https://doi.org/10.1084/jem.20110551

Zamani, F.; Samiei, F.; Mousavi, Z.; Azari, M.R.; Seydi, E. and Pourahmad, J. (2021): Apigenin ameliorates oxidative stress and mitochondrial damage induced by multiwall carbon nanotubes in rat kidney mitochondria. *J. Biochem. Mol. Toxicol.* 2021, *35*, 1–7. [Google Scholar] [CrossRef] [PubMed]

Zhang, Z.; Mi, T.; Jin, L.; Li, M.; Zhanghuang, C.; Wang, J.; Tan, X.; Lu, H.; Shen, L.; Long, C.; Wei, G. and He, D. (2022): Comprehensive proteomic analysis of exosome mimetic vesicles and exosomes derived from human umbilical cord mesenchymal stem cells. *Stem Cell Research & Therapy*, *13*(1). https://doi.org/10.1186/s13287-022-03008-6

Zheng, Y.; Liu, J.; Chen, P.; Lin, L.; Luo, Y. and Ma, X. et al. (2021): Exosomal miR-22-3p from human umbilical cord blood-derived mesenchymal stem cells protects against

lipopolysaccharid-induced acute lung injury. Life Sci (2021) 269:119004. doi: 10.1016/j.lfs.2020.119004

Zhong, Z.; Umemura, A.; Sanchez-Lopez, E.; Liang, S.; Shalapour, S.; Wong, J.; He, F.; Boassa, D.; Perkins, G. and Ali, S.R., et al. (2016): NF-κB restricts inflammasome activation via elimination of damaged mitochondria. Cell, 164(5), 896–910. https://doi.org/10.1016/j.cell.2015.12.057

Zhou, J.; Lin, Y.; Kang, X.; Liu, Z.; Zhang, W. and Xu, F. (2021): MicroRNA-186 in extracellular vesicles from bone marrow mesenchymal stem cells alleviates idiopathic pulmonary fibrosis via interaction with SOX4 and DKK1. Stem Cell Res Therapy. 2021;12(1).

تقييم التأثير التحسيني للخلايا الجذعية الوسيطة /الميزنكيمية والإكسوسومات على سمّية الرئة الناتجة عن الأنابيب النانوية الكربونية متعددة الجدران باستخدام الدراسات الباثولوجية والتحليل المورفومتري في الجرذان

نهير احمد محمود محمد ، محمود بدوي محمد البجاوي ، ولاء عبد الرحمن مصيلحي عبد القادر ، دعاء رمضان إسماعيل عبد الجواد ، الشيماء نبيل احمد النحاس

Email: nohairmohamed841_sd@vet.b-su.edu.eg
Assiut University web-site: www.aun.edu.eg

أثار الاستخدام المتزايد للأنابيب النانوية الكربونية متعددة الجدران في الصناعة والطب مخاوف بشأن سُمّيتها المحتملة على صحة الإنسان والحيوان، خاصة قدرتها على إحداث الإجهاد التأكسدي والالتهاب والتليّف. وفي هذا السياق، تم في الدراسة الحالية تقييم تأثير الخلايا الجذعية المتوسطة/ الميزنكيمية وإكسوسوماتها ضد السُمية الرئوية الناتجة عن التعرض لأنابيب النانوية الكربونية متعددة الجدران في ذكور الجرذان البيضاء.

شملت الدراسة ٣٢ جرذًا ذكرًا بعمر ٤ أسابيع، وُزّعوا إلى أربعة مجموعات:

١) مجموعة ضابطة تلقت محلولًا ملحيًا عاديًا.

٢) مجموعة تعرضت لأنابيب النانوية الكربونية متعددة الجدران بجرعة ١ مجم/كجم من وزن الجسم عن طريق الحقن داخل الصفاق (IP) مرتين خلال الأسبوعين الأول والثالث.

٣) مجموعة تعرضت لأنابيب النانوية الكربونية متعددة الجدران بالإضافة إلى الخلايا الجذعية الميزنكيمية والإكسوسومات، حيث تلقت الجرذان الانابيب النانوية الكربونية متعددة الجدران بالجرعة نفسها تلاها حقن أسبوعيا بالخلايا الجذعية (٢,٥ × 10^6 خلية/كجم) والإكسوسومات (١٠٠ ميكروجرام من بروتين مشتقات الخلايا الجذعية/كجم) لمدة ثلاثة أسابيع.

٤) مجموعة تلقت الخلايا الجذعية والإكسوسومات فقط دون التعرض لأنابيب النانوية الكربونية متعددة الجدران وبذات الجرعات.

أدى التعرض لأنابيب النانوية الكربونية متعددة الجدران إلى زيادة ملحوظة في سُمك الظهارة القصيبية، وتضخم خلايا الكأس، وارتفاع مستويات التليف (وفقًا لصبغه ماسون ثلاثية الالوان)، وزيادة مؤشرات الإجهاد التأكسدي مثل المالونديالديهيد (MDA). وقد ساهمت المعالجة بالخلايا الجذعية والإكسوسومات في التخفيف من هذه التأثيرات من خلال تقليل سُمك الظهارة وتضخم خلايا الكأس، وخفض التليف، واستعادة مؤشرات مضادات الأكسدة مثل الجلوتاثيون.

تُبرز هذه النتائج الفعالية العلاجية للخلايا الجذعية الميزنكيمية، وأهمية أدوات علم الامراض الرقمي في أبحاث سمّية النانو مثل ImageJ .

الكلمات المفتاحية:
الأنابيب النانوية الكربونية متعددة الجدران، إكسوسومات مشتقة من الخلايا الجذعية، التحليل المورفومتري، السُمية الرئوية ImageJ,